Dynamics of a Soft Contractile Body on a Hard Support

A. Tatone, A. Di Egidio and A. Contento

Abstract The motion of a soft and contractile body on a hard support is described by fields of short range contact forces. Besides repulsion these forces are able to describe also viscous friction, damping and adhesion allowing the body to have complex motions which look rather realistic. The contractility is used to make the body behave like a living body with some basic locomotion capabilities. The simulated motions, showing jumping or crawling, are driven either by a contraction or by a contractile couple. Although only homogeneous deformations are allowed, the model arises from a general theory of remodeling in finite elasticity. The body is made of a viscoelastic incompressible neo-Hookean material.

1 Introduction

The aim of this paper is to use a contact model to describe the complex motions of stiff, soft and contractile bodies interacting with a rigid flat support. The body model, though restricted to homogeneous deformations, is derived from a general continuum theory of remodeling in finite elasticity, as set up in [3, 7]. A summary of that theory is given in sections 2 and 3. The body is made of a viscoelastic incompressible neo-Hookean material.

Contractility is the ability of bodies, like muscle cells and fibres to contract or to extend in order to apply forces. More precisely, it can be defined as the ability to modify the zero stress, or relaxed, configuration [11]. Contractility can also give an elementary body some motility and locomotion capabilities allowing it to move over a substrate [14, 9]. The simulated motions described here, showing jumping or crawling, are driven either by a contraction or by a contractile couple.

We use a contact model described by constitutive laws for the contact forces arising from the interaction of the body boundary and the support surface, which

Department of Structural, Hydraulic and Geotechnical Engineering, University of L'Aquila, L'Aquila, Italy, e-mail: amabile.tatone@univaq.it

get close to each other during a motion, without enforcing explicitly unilateral constraints, in the spirit of [15], chap. 5. An interatomic potential was used in [8, 10, 6] to add adhesion to the Hertz model, and in contact modeling based on molecular dynamics, as in [4]. In macroscopic modeling the interatomic potential is replaced by a surface contact potential, as in [16, 1] and more recently discussed in [12, 13].

The contact tractions on the body boundary are given here by four short range force fields of different kind, potential or dissipative, all of them depending on the distance from the support: i) a repulsive force field; ii) an adhesive force field, both derived from a Lennard-Jones–like surface contact potential; iii) a damping force field, describing the impact dissipation and depending on the normal velocity; iv) a viscous frictional force field, depending on the sliding velocity. They decay very fast as the distance increases and grow to infinity as the body and the support get closer and closer. Hence the body will never *touch* the support. Instead, the true *contact distance* will depend on the motion, although some characteristic values can be related to the constitutive properties of each contact force field.

Although the law used for the frictional force field does not implement a Coulomb like friction, the two dissipation mechanisms iii) and iv) turn out to be suitable to describe the dynamical behavior of a body over a support.

Summarizing, this paper briefly shows how a simple model can be defined within the context of finite elasticity and contact mechanics, including all the details needed to set up numerical physics-based simulations, showing a body bouncing and rolling and even crawling over a flat rigid support.

Though the simulations do not make use of experimental data for the material properties of neither the body nor the substrate, they seem useful to provide some insight into the dynamics of a simple body over a substrate and the mechanisms on which locomotion could be based.

2 Affine Contractile Body

The motion of a body $\mathscr{B}$ is described by a mapping

$$\mathbf{p} : \mathscr{D} \times \mathscr{I} \to \mathscr{E}\,, \tag{1}$$

transforming the *reference shape* $\mathscr{D}$, at each time $t \in \mathscr{I}$, into the *current shape* $\mathbf{p}(\mathscr{D},t)$ in a three-dimensional Euclidean space $\mathscr{E}$. An *affine* or *homogeneous* motion is completely defined at any time t by the current position $\mathbf{p}_0(t)$ of a point occupying a position $\mathbf{x}_0$ in $\mathscr{D}$ and by the *deformation gradient* $\nabla\mathbf{p}(t)$, with $\det\nabla\mathbf{p}(t) > 0$, through the following representation

$$\mathbf{p}(\mathbf{x},t) = \mathbf{p}_0(t) + \nabla\mathbf{p}(t)(\mathbf{x}-\mathbf{x}_0)\,, \quad \forall\mathbf{x} \in \mathscr{D}\,. \tag{2}$$

As a consequence, an affine velocity field $\mathbf{v}$ at any time t has the representation

$$\mathbf{v}(\mathbf{x}) = \mathbf{v}_0 + \nabla\mathbf{v}\,(\mathbf{x}-\mathbf{x}_0)\,, \tag{3}$$

where $\nabla\mathbf{v}$ is the velocity gradient. Along the motion (2) at time t

$$\nabla\mathbf{v} = \nabla\dot{\mathbf{p}}(t)\,, \quad \mathbf{v}_0 = \dot{\mathbf{p}}_0(t)\,, \tag{4}$$

where the dot denotes time derivatives.

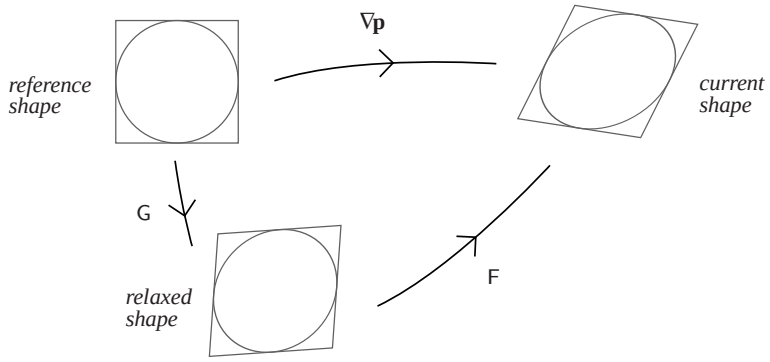

Fig. 1 Kröner-Lee decomposition of the deformation gradient $\nabla\mathbf{p}$.

In order to describe *contractility* we introduce a new tensor $\mathsf{G}(t)$, such that $\det\mathsf{G}(t) > 0$, transforming the reference shape $\mathscr{D}$ into a *relaxed shape* at time t, and will assume that the strain energy is a function of F as defined by the Kröner-Lee decomposition (see Fig. 1)

$$\mathsf{F}(t) := \nabla\mathbf{p}(t)\,\mathsf{G}(t)^{-1}\,. \tag{5}$$

Let us denote by V the velocity corresponding to G which takes the value

$$\mathsf{V} = \dot{\mathsf{G}}(t)\,\mathsf{G}(t)^{-1} \tag{6}$$

at time t along a motion described by $(\mathbf{p},\mathsf{G})$. We assume as *balance principle* (following [5]) that at any time t for any test velocity field $(\mathbf{v},\mathsf{V})$

$$\begin{aligned}\int_{\mathscr{D}} \mathbf{b}(\mathbf{x},t)\cdot\mathbf{v}\,\mathrm{d}V + \int_{\partial\mathscr{D}} \mathbf{q}(\mathbf{x},t)\cdot\mathbf{v}\,\mathrm{d}A \\ - \mathsf{S}(t)\cdot\nabla\mathbf{v}\,\mathrm{vol}\,(\mathscr{D}) + \big(\mathsf{Q}(t) - \mathsf{A}(t)\big)\cdot\mathsf{V}\,\mathrm{vol}\,(\mathscr{D}) = 0\,,\end{aligned} \tag{7}$$

where the bulk density force $\mathbf{b}$, denoting by ρ the reference mass density, is composed of the inertial force and the gravity force densities

$$\mathbf{b}(\mathbf{x},t) := -\rho(\mathbf{x})\left(\ddot{\mathbf{p}}(\mathbf{x},t) + \mathbf{g}\right), \tag{8}$$

while the traction $\mathbf{q}$ on the boundary is assumed to be the sum of different contact force fields $\mathbf{q}_j$. The tensor $\mathsf{S}(t)$ is the Piola stress in the reference shape, related to

the Cauchy stress T by

$$\mathsf{T} = \mathsf{S}\nabla\mathbf{p}^{\mathsf{T}}(\det\nabla\mathbf{p})^{-1}. \tag{9}$$

The tensors $\mathsf{A}(t)$ and $\mathsf{Q}(t)$ are the *internal* and *external contractile couples* per unit reference volume. The first one describes the material response while the second one describes an action from outside the mechanical system, which could be controlled by an electrical or biochemical signal.

The balance equations corresponding to (7) turn out to be

$$-m\ddot{\mathbf{p}}_0(t) - m\mathbf{g} + \mathbf{f}(t) = 0\,, \tag{10}$$

$$-\nabla\ddot{\mathbf{p}}(t)\,\mathsf{E} + \mathsf{M}(t) - \mathsf{S}(t)\,\mathrm{vol}\,(\mathscr{D}) = 0\,, \tag{11}$$

$$\mathsf{Q}(t) - \mathsf{A}(t) = 0\,. \tag{12}$$

The scalar quantity m is the total mass $\int_{\mathscr{D}}\rho\,\mathrm{d}V$, while E is the Euler tensor

$$\mathsf{E} := \int_{\mathscr{D}}\rho(\mathbf{x})(\mathbf{x}-\mathbf{x}_0)\otimes(\mathbf{x}-\mathbf{x}_0)\,\mathrm{d}V\,, \tag{13}$$

where $\mathbf{x}_0$ has been chosen as the barycenter of $\mathscr{D}$. The contact force fields $\mathbf{q}_j$ give rise to the total force

$$\mathbf{f}(t) := \sum_j \int_{\partial\mathscr{D}} \mathbf{q}_j(\mathbf{x},t)\mathrm{d}A \tag{14}$$

and to the total moment tensor[1]

$$\mathsf{M}(t) := \sum_j \int_{\partial\mathscr{D}} (\mathbf{x}-\mathbf{x}_0)\otimes\mathbf{q}_j(\mathbf{x},t)\mathrm{d}A\,. \tag{15}$$

The volume of the reference shape is denoted by $\mathrm{vol}\,(\mathscr{D})$.

3 Dissipation Inequality and Material Characterization

The material response can be characterized (as in [3] and [7]) by assuming that along any motion at any time t

$$\mathsf{A}\cdot\dot{\mathsf{G}}\mathsf{G}^{-1} + \mathsf{S}\cdot\nabla\dot{\mathbf{p}} - \frac{d}{dt}\big(J\,\varphi(\mathsf{F})\big) \geq 0\,, \tag{16}$$

where φ is the *strain energy density* per unit relaxed volume and $J := \det\mathsf{G}$. Note that, because of the balance principle (7), the power $(\mathsf{A}\cdot\dot{\mathsf{G}}\mathsf{G}^{-1} + \mathsf{S}\cdot\nabla\dot{\mathbf{p}})$ equals the

[1] Here we use the following definition of tensor product:

$$(\mathbf{u}\otimes\mathbf{f})\,\mathbf{e} = (\mathbf{u}\cdot\mathbf{e})\mathbf{f} \quad \forall\mathbf{e}\,.$$

power, per unit reference volume, of the bulk forces, the contact forces and the external contractile couple. Thus the dissipation principle above states that the external power is not entirely balanced by a rate of change of the strain energy. By replacing $\nabla\dot{\mathbf{p}}$ with the time derivative of the Kröner-Lee decomposition of $\nabla\mathbf{p}$ defined in (5), we get

$$\mathsf{A}\cdot\dot{\mathsf{G}}\mathsf{G}^{-1}+\mathsf{S}\mathsf{G}^{\mathsf{T}}\cdot\dot{\mathsf{F}}+\mathsf{F}^{\mathsf{T}}\mathsf{S}\mathsf{G}^{\mathsf{T}}\cdot\dot{\mathsf{G}}\mathsf{G}^{-1}-J\frac{d}{dt}\varphi(\mathsf{F})-J\,\varphi(\mathsf{F})\mathsf{I}\cdot\dot{\mathsf{G}}\mathsf{G}^{-1}\geq 0\,. \tag{17}$$

Since $d\,\varphi(\mathsf{F})/dt$ is linear in $\dot{\mathsf{F}}$, we can define the *elastic response* for the Piola stress $\mathbb{S}:=J^{-1}\mathsf{S}\mathsf{G}^{\mathsf{T}}$, *pull-back* of T to the relaxed shape, as the function $\widehat{\mathbb{S}}$ such that in any motion

$$\widehat{\mathbb{S}}(\mathsf{F})\cdot\dot{\mathsf{F}}=\frac{d}{dt}\varphi(\mathsf{F})\,. \tag{18}$$

By requiring φ to be frame-indifferent it turns out that the Cauchy stress (9) is a symmetric tensor. Going back to (17), after substituting (18) we can collect all terms in two groups

$$\big(\mathsf{S}-\widehat{\mathsf{S}}(\mathsf{F})\big)\nabla\mathbf{p}^{\mathsf{T}}\cdot\dot{\mathsf{F}}\mathsf{F}^{-1}+\big(\mathsf{A}+\mathsf{F}^{\mathsf{T}}\mathsf{S}\mathsf{G}^{\mathsf{T}}-J\,\varphi(\mathsf{F})\mathsf{I}\big)\cdot\dot{\mathsf{G}}\mathsf{G}^{-1}\geq 0 \tag{19}$$

with $\widehat{\mathbb{S}}(\mathsf{F})=J^{-1}\widehat{\mathsf{S}}(\mathsf{F})\mathsf{G}^{\mathsf{T}}$. Setting

$$\begin{aligned}\mathsf{S}^{+}&:=\mathsf{S}-\widehat{\mathsf{S}}(\mathsf{F})\,,\\ \mathsf{A}^{+}&:=\mathsf{A}+\mathsf{F}^{\mathsf{T}}\mathsf{S}\mathsf{G}^{\mathsf{T}}-J\,\varphi(\mathsf{F})\mathsf{I}\,,\end{aligned} \tag{20}$$

the dissipation inequality (19) takes the form

$$\mathsf{S}^{+}\nabla\mathbf{p}^{\mathsf{T}}\cdot\dot{\mathsf{F}}\mathsf{F}^{-1}+\mathsf{A}^{+}\cdot\dot{\mathsf{G}}\mathsf{G}^{-1}\geq 0\,. \tag{21}$$

In order for S^{+} and A^{+} to satisfy a-priori the dissipation inequality (21) both of them have to depend on $\dot{\mathsf{F}}\mathsf{F}^{-1}$ and $\dot{\mathsf{G}}\mathsf{G}^{-1}$. A possible constitutive prescription, recovering the classical viscous stress, consists in assuming

$$\begin{aligned}\mathsf{S}^{+}\nabla\mathbf{p}^{\mathsf{T}}&=\mu\,\mathrm{sym}\,(\dot{\mathsf{F}}\mathsf{F}^{-1})\,,\\ \mathsf{A}^{+}&=\mu_{\gamma}\dot{\mathsf{G}}\mathsf{G}^{-1}\,,\end{aligned} \tag{22}$$

with positive scalars μ, the *viscosity*, and μ_{γ}, the *resistance to contraction*.

Hence A and S are constitutively characterized by the expressions

$$\begin{aligned}\mathsf{S}&=\mathsf{S}^{+}+\widehat{\mathsf{S}}(\mathsf{F})=\mu\,\mathrm{sym}\,(\dot{\mathsf{F}}\mathsf{F}^{-1})\nabla\mathbf{p}^{-\mathsf{T}}+\widehat{\mathsf{S}}(\mathsf{F})\,,\\ \mathsf{A}&=\mathsf{A}^{+}-\mathsf{F}^{\mathsf{T}}\mathsf{S}\mathsf{G}^{\mathsf{T}}+J\,\varphi(\mathsf{F})\mathsf{I}=\mu_{\gamma}\dot{\mathsf{G}}\mathsf{G}^{-1}-\mathsf{F}^{\mathsf{T}}\mathsf{S}\mathsf{G}^{\mathsf{T}}+J\,\varphi(\mathsf{F})\mathsf{I}\,.\end{aligned} \tag{23}$$

Now the balance equation (12) takes the form of an evolution equation

$$\mu_{\gamma}\dot{\mathsf{G}}\mathsf{G}^{-1}=\mathsf{F}^{\mathsf{T}}\mathsf{S}\mathsf{G}^{\mathsf{T}}-J\,\varphi(\mathsf{F})\mathsf{I}+\mathsf{Q}\,, \tag{24}$$

where S is meant to be given by the first of (23). The external contractile couple Q is the driving force, which could be related to some other quantity like an electrical or biochemical signal. In some of the simulations shown in this paper the motion is driven by G instead. In those cases Q is just a reactive contractile couple given by (24). We will consider an incompressible material defined by the neo-Hookean strain energy function

$$\varphi(\mathsf{F}) := c_1(\imath_1(\mathsf{C}) - 3)\,, \tag{25}$$

where c_1 is the elastic moduli and $\imath_1(\mathsf{C})$ is the trace of the Cauchy–Green tensor $\mathsf{C} := \mathsf{F}^{\mathsf{T}}\mathsf{F}$. Because of the incompressibility constraint $\det\mathsf{F} = 1$, the velocity fields turn out to be isochoric, i.e. such that $\mathrm{tr}\dot{\mathsf{F}}\mathsf{F}^{-1} = 0$. Hence there exists a *reactive* spherical part $-\pi\mathsf{I}$ of S, while the inequality (19) characterizes only the deviatoric part S_0. Thus the first of (23) will be replaced by

$$\mathsf{S} = \mu\ \mathrm{sym}\,(\dot{\mathsf{F}}\mathsf{F}^{-1})\nabla\mathbf{p}^{-\mathsf{T}} + \widehat{\mathsf{S}}_0(\mathsf{F}) - \pi\nabla\mathbf{p}^{-\mathsf{T}}\,. \tag{26}$$

4 Surface Energy and Contact Force Characterization

The flat surface $\mathscr{S}$ of the rigid support can be defined by the position $\mathbf{o}$ of a point on it and by the exterior unit normal vector $\mathbf{n}$. The distance of a point $\mathbf{x}$ on $\partial\mathscr{D}$ from $\mathscr{S}$ at time t is

$$d(\mathbf{x},t) := (\mathbf{p}(\mathbf{x},t) - \mathbf{o})\cdot\mathbf{n}\,, \tag{27}$$

where $\mathbf{p}(\mathbf{x},t)$ is the position occupied by $\mathbf{x}$ at time t.

In order to describe the contact interaction it is convenient to consider the body and the support as a whole body and to define a *surface contact potential* ψ as a density per unit reference area on $\partial\mathscr{D}$. If we assume that this potential depends only on the distance d it turns out to be frame-indifferent. Accordingly, the dissipation inequality (16) should be changed into

$$\begin{aligned}\mathrm{vol}\,(\mathscr{D})\big(\mathsf{A}\cdot\dot{\mathsf{G}}\mathsf{G}^{-1} + \mathsf{S}\cdot\nabla\dot{\mathbf{p}}\big) - \int_{\partial\mathscr{D}}\mathbf{q}\cdot\dot{\mathbf{p}}\,\mathrm{d}A\\ -\mathrm{vol}\,(\mathscr{D})\frac{d}{dt}\big(J\,\varphi(\mathsf{F})\big) - \frac{d}{dt}\int_{\partial\mathscr{D}}\psi(d)\,\mathrm{d}A \geq 0\,,\end{aligned} \tag{28}$$

where the terms in the first row, through (7), equal the power of the external bulk forces and the external contractile couple. This condition can be replaced by the stronger requirement that (16) be satisfied together with the following condition

$$-\mathbf{q}(\mathbf{x},t)\cdot\dot{\mathbf{p}}(\mathbf{x},t) - \frac{d}{dt}\psi(d(\mathbf{x},t)) \geq 0 \quad \forall\mathbf{x}\in\partial\mathscr{D} \tag{29}$$

Since the rate of change of the contact potential is linear in $\dot{d} = \mathbf{n}\cdot\dot{\mathbf{p}}$, we can define the *potential contact force* through a scalar field $\hat{q}$ such that in any motion

$$\hat{q}(\mathbf{x},t)\,\mathbf{n}\cdot\dot{\mathbf{p}}(\mathbf{x},t) = -\frac{d}{dt}\psi(d(\mathbf{x},t))\,, \tag{30}$$

which allows (29) to be rewritten as

$$-\big(\mathbf{q}(\mathbf{x},t) - \hat{q}(\mathbf{x},t)\,\mathbf{n}\big)\cdot\dot{\mathbf{p}}(\mathbf{x},t) \geq 0 \quad \forall \mathbf{x}\in\partial\mathscr{D}\,, \tag{31}$$

or simply

$$-\mathbf{q}^{+}(\mathbf{x},t)\cdot\dot{\mathbf{p}}(\mathbf{x},t) \geq 0\,, \tag{32}$$

with $\mathbf{q}^{+}(\mathbf{x},t) := (\mathbf{q}(\mathbf{x},t) - \hat{q}(\mathbf{x},t)\,\mathbf{n})$ *the dissipative contact force*. The requirement above is a restriction on constitutive laws for contact forces.

5 Contact Constitutive Laws

The *repulsive* traction field is assumed to be defined on $\partial\mathscr{D}$ by a surface potential

$$\psi_{\mathfrak{r}}(d(\mathbf{x},t)) := \frac{\alpha_{\mathfrak{r}}}{\nu_{\mathfrak{r}}-1}\,d(\mathbf{x},t)^{-\nu_{\mathfrak{r}}+1}\,. \tag{33}$$

where the coefficient $\alpha_{\mathfrak{r}}$ is a positive real number and the exponent $\nu_r > 1$ is an integer. The corresponding constitutive law, through (30), turns out to be

$$\mathbf{q}_{\mathfrak{r}}(\mathbf{x},t) = \alpha_{\mathfrak{r}}\; d(\mathbf{x},t)^{-\nu_{\mathfrak{r}}}\,\mathbf{n}\,, \tag{34}$$

A value for $\alpha_{\mathfrak{r}}$ can be obtained by requiring the repulsive force to balance the gravity force when the body stays at rest at an equilibrium distance d_0 from a horizontal surface, thus relating $\alpha_{\mathfrak{r}}$ to a characteristic distance.

An impact dissipation can be described by the following *damping* traction on $\partial\mathscr{D}$

$$\mathbf{q}_{\mathfrak{d}}(\mathbf{x},t) = -\beta_{\mathfrak{d}}\; d(\mathbf{x},t)^{-\nu_{\mathfrak{d}}}\,(\mathbf{n}\otimes\mathbf{n})\,\dot{\mathbf{p}}(\mathbf{x},t)\,, \tag{35}$$

where the damping factor $\beta_{\mathfrak{d}}$ is a positive real number and $\nu_{\mathfrak{d}}$ a positive integer. The tensor $(\mathbf{n}\otimes\mathbf{n})$ is the projector onto the direction orthogonal to $\mathscr{S}$.

The simulations shown in this paper make use of a viscous *friction* defined by the following constitutive law

$$\mathbf{q}_{\mathfrak{f}}(\mathbf{x},t) = -\beta_{\mathfrak{f}}\; d(\mathbf{x},t)^{-\nu_{\mathfrak{f}}}\,\dot{\mathbf{p}}_{\tau}(\mathbf{x},t)\,, \tag{36}$$

which is linear in the tangent velocity projection $\dot{\mathbf{p}}_{\tau}(\mathbf{x},t) := (\mathsf{I}-\mathbf{n}\otimes\mathbf{n})\,\dot{\mathbf{p}}(\mathbf{x},t)$ and depends also on d. The coefficient $\beta_{\mathfrak{f}}$ is a positive real number and $\nu_{\mathfrak{f}}$ is a positive integer. If we allow $\beta_{\mathfrak{f}}$ not to be a constant we could also use the following law

$$\mathbf{q}_{\mathfrak{f}_C}(\mathbf{x},t) = -\alpha_{\mathfrak{r}}\; d(\mathbf{x},t)^{-\nu_{\mathfrak{r}}}\,\mu_{\mathfrak{f}}(\|\dot{\mathbf{p}}_{\tau}(\mathbf{x},t)\|)\,\frac{\dot{\mathbf{p}}_{\tau}(\mathbf{x},t)}{\|\dot{\mathbf{p}}_{\tau}(\mathbf{x},t)\|}\,. \tag{37}$$

This expression could be given the form of a regularized Coulomb law ([15], chap. 5) depending on the repulsive traction (34) and on a regular positive function $\mu_{\mathfrak{f}}$ of the tangent velocity. In some of the following simulations adhesion will be introduced through an additional potential contact force which is given the following law

$$\mathbf{q}_{\mathfrak{a}}(\mathbf{x},t) = \left(\beta_{\mathfrak{r}}\, d(\mathbf{x},t)^{-\nu_{\mathfrak{r}}} - \beta_{\mathfrak{a}}\, d(\mathbf{x},t)^{-\nu_{\mathfrak{a}}}\right) \mathbf{n}\,, \tag{38}$$

where $\beta_{\mathfrak{r}}$ and $\beta_{\mathfrak{a}}$ are positive real numbers and $\nu_{\mathfrak{a}}$ is a positive integer.

It is worth noting that the condition that $\beta_{\mathfrak{d}}$, $\beta_{\mathfrak{f}}$, $\mu_{\mathfrak{f}}$ be positive makes each of the above constitutive laws for the dissipative traction fields $\mathbf{q}_{\mathfrak{d}}$, $\mathbf{q}_{\mathfrak{f}}$, $\mathbf{q}_{\mathfrak{f}_C}$ fulfill separately the requirement (32).

6 Contact Force Distributions

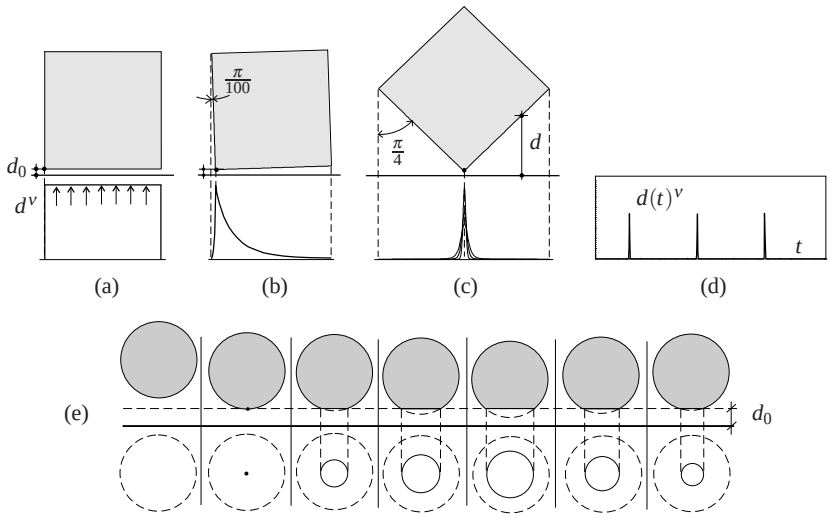

Fig. 2 (a) Spatial distribution of the function $d^{-\nu}$, with $d_0 = 0.01$ and lower face parallel to the support surface; (b) body rotated by $\vartheta = \pi/100$ about the left lower edge; (c) body rotated by $\vartheta = \pi/4$. (d) Time evolution of the function $d^{-\nu}$ at the bottom edge during an undamped vertical bouncing motion, with $\vartheta = \pi/4$. (e) Different frames of a bouncing rigid sphere and sections at distance d_0.

In order to illustrate the role of the parameters on which the contact tractions depend, it could useful to recall some elementary properties. All of the traction fields given by (34)-(38) depend on the function $d^{-\nu}$. Figures 2 (a)-(b)-(c) show how rapidly the graph of $d^{-\nu}$ changes when rotating a body in the shape of a cube around an edge: when the lower face of the body is parallel to the support $\mathscr{S}$ (Fig. 2 a), the graph is flat; as soon as the body rotates by a very small angle (Fig. 2 b) the graph

rapidly decreases from a maximum value attained at the edge; when the body is in the unstable equilibrium configuration (Fig. 2 c) the graph becomes very sharp: the higher the value of the exponent ν the sharper the graph. Finally, figure 2 (d) shows the time evolution of the function $d^{-\nu}$ at the edge close to the support, when the body bounces vertically.

Even though the support does not deform and the body never touches its surface, we can consider the cross section of the body shape at a characteristic distance d_0 from the support as a "contact area". In Fig. 2 (d), different frames of a bouncing rigid sphere are shown together with the corresponding contact cross sections.

7 Numerical Simulations

7.1 Parameter Choice and Computational Details

Several numerical simulations have been performed using different constitutive parameters and different initial conditions. The whole boundary of the body was supposed to be able to interact with the support surface, with uniform properties. The body has a nonzero uniform mass density and is subjected to a downward gravity field, while the support is rigid, flat and usually horizontal.

All the simulations were aimed at testing the ability of both the body model and the contact model to exhibit a somewhat "qualitatively realistic" behavior. By this we mean the ability of bouncing and rolling, and also jumping and crawling, within a time interval of few seconds, with a length scale of 1 m, a mass density of about $10^3\,\mathrm{kg/m^3}$, an elastic modulus around 1 MPa. Calibration of the parameters was done to this end. No comparison was made with experimental data. That is why the presented simulations do not constitute a quantitative benchmark set. Some simulations of a three-dimensional motion of a rigid body can be found in [2].

The computational scheme can shortly be described as follows: the main procedure consists in the numerical integration of the equations of motion (10), (11), (12) starting from given initial conditions. For plane motions, the number of corresponding scalar time differential equations is 2 for eqn. (10), 4 for eqn. (11), and 4 for eqn. (24) which is the explicit form of eqn. (12). At a lower level, for each time step, the main task consists in computing the integrals (14) and (15) over the boundary $\partial\mathscr{D}$. The whole procedure has been implemented in *Mathematica*®, which has also been used to derive the general expressions for each of the traction fields in sect. 4, starting from the motion description (2) and making use of (7). The time integration, as well as the integration on the boundary, has been performed by using the Mathematica built-in functions with only some parameter tweaking.

The outcome of each time integration, after a dump of the Mathematica session, was routinely processed producing graphs and movies.

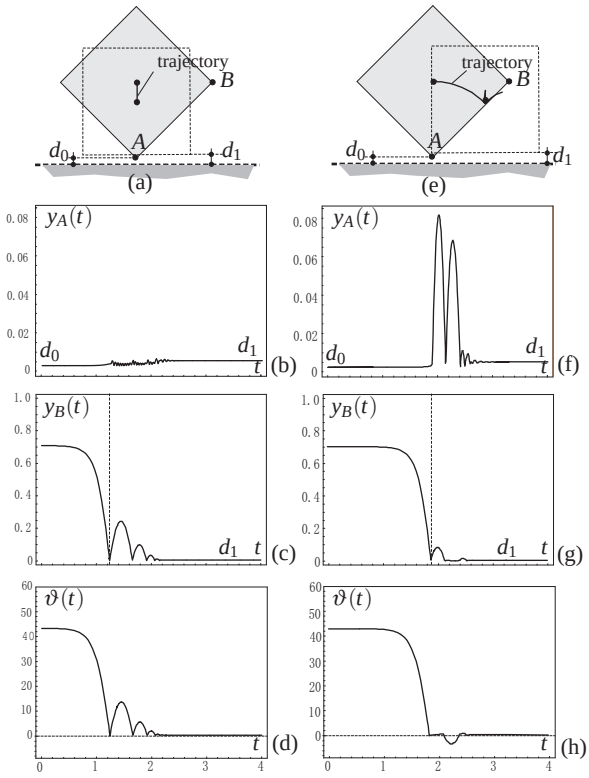

Fig. 3 Plane motion of a rigid body in the shape of a cube. Left column: contact without friction ($L = 1\,\mathrm{m}$, $d_0 = 0.002\,\mathrm{m}$, $v_0 = 0$, $\vartheta_0 = 0.99\,\pi/4$, $\nu_\mathfrak{r} = 8$, $\rho = 10^3\,\mathrm{kg/m^3}$, $\nu_\mathfrak{d} = 2$, $\beta_\mathfrak{d}/d_0^{\nu_\mathfrak{d}} = 2.5 \times 10^5\,\mathrm{Pa\,s/m}$, $\beta_\mathfrak{f} = 0$). Right column: contact with friction ($\nu_\mathfrak{f} = 2$, $\beta_\mathfrak{f}/d_0^{\nu_\mathfrak{f}} = 2.5 \times 10^7\,\mathrm{Pa\,s/m}$); (a)-(e) initial and final configurations and trajectory of the center; (b)-(f) distance of A from the support; (c)-(g) distance of B from the support; (d)-(h) rotation amplitude.

7.2 Sliding, Bouncing and Rocking

Figure 3 shows the plane motion of a rigid body in the shape of a cube, with edge length L, starting from a slightly perturbed unstable equilibrium configuration. The left column (a)-(d) refers to a contact without friction, while the right column (e)-(h) refers to a contact with friction. The graphs show the time evolution of the distances $y_A(t)$ and $y_B(t)$ of the A and B edges from the support, together with the time evolution of the rotation amplitude $\vartheta(t)$. Both the initial configurations (gray) and the limit configurations (dashed) can be seen at the top of the figure. Looking at the left column (Fig. 3 b-c) we can see how the edge A changes only slightly its distance from the support, while the edge B falls down in a clockwise rotation of the body (Fig. 3 d) until it starts bouncing. Both A and B edges reach, in a long enough time span, the same distance from the support, slightly greater than the initial one be-

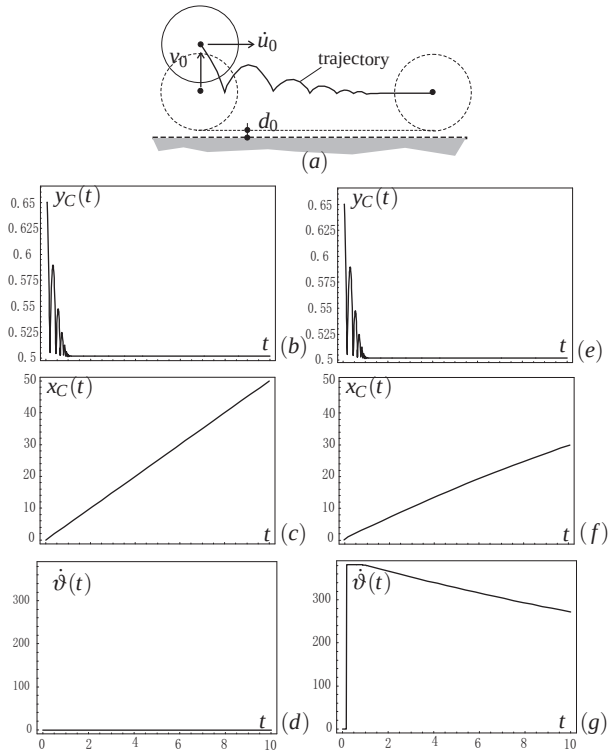

Fig. 4 Plane motion of a rigid circular cylinder. Left column: contact without friction ($L = 1\,\mathrm{m}$, $d_0 = 0.002\,\mathrm{m}$, $v_0 = 0.15\,\mathrm{m}$, $\dot{u}_0 = 5\,\mathrm{m/s}$, $\nu_\mathfrak{r} = 8$, $\rho = 10^3\,\mathrm{kg/m^3}$, $\nu_\mathfrak{d} = 4$, $\beta_\mathfrak{d}/d_0^{\nu_\mathfrak{d}} = 6.25\times10^5\,\mathrm{Pa\,s/m}$, $\beta_\mathfrak{f} = 0$). Right column: contact with friction ($\nu_\mathfrak{f} = 6$, $\beta_\mathfrak{f}/d_0^{\nu_\mathfrak{f}} = 1.6\times10^{19}\,\mathrm{Pa\,s/m}$).

cause the body ends up lying on a flat face instead of an edge. This fact, together with the small oscillations the edge A exhibits in the transition (Fig. 3 b), reveals the absence of a real contact surface. When frictional forces are added, the system exhibits a richer dynamics.

As can be seen from the bouncing of both edges A and B (Fig. 3 f-g), the rigid motion resembles a rocking motion until it fades out. In the frictionless case (Fig. 3 a) the trajectory of the center of the rigid body turns out to be vertical. That means that while the body rotates, the edge A slides leftward. Instead, if the friction coefficient is large enough the edge A does not slide any more, though it bounces for a while (Fig. 3 e-g), thus making the trajectory of the center very different from the previous case and even longer. These differences could be caught also by comparing the first impact time (Fig. 3 c-g).

7.3 Bouncing and Rolling

Figure 4 shows the plane motion of a rigid body in the shape of a circular cylinder, with diameter L, which drops on the support from a distance v_0 with initial horizontal velocity $\dot{u}_0$. The left column (b)-(d) refers to a contact without friction, while the right column (e)-(g) refers to a contact with friction. Graphs (b)-(e) and (c)-(f) show the time evolution of the vertical and horizontal coordinates of the center, $y_C(t)$ and $x_C(t)$, while graphs (d)-(g) show the time evolution of the angular velocity. The trajectory of the center drawn in the top panel (a) has been rescaled to make the bouncing more visible. Although friction does not affect the time evolution of the distance of the center from the support (the vertical motion of the body), as can be seen comparing Fig. 4 (b) and Fig. 4 (e), it makes the motion quite different: at the first impact the angular velocity rises suddenly (Fig. 4 g), as a consequence of the initial value of the horizontal velocity. That means that the friction makes the cylinder roll while, at the same time, lowering the horizontal velocity (compare Fig. 4 (f) and Fig. 4 (c)). Finally, it is worth to note how the angular velocity decreases after the bouncing has faded out. This is a consequence of the damping forces (35) acting on points close to the contact, whose vertical velocity is different from zero because of rolling.

7.4 Adhesion and Detachment

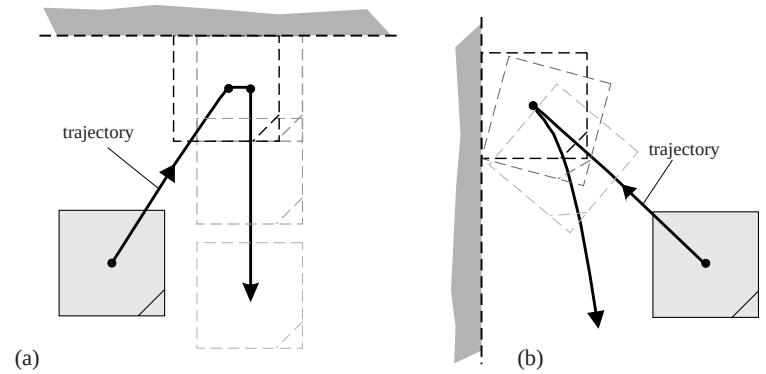

Fig. 5 Effect of the adhesive forces: (a) adhesion to a ceiling; (b) adhesion to a vertical wall; ($L = 1\,\mathrm{m}$, $d_0 = 0.002\,\mathrm{m}$, $\nu_{\mathfrak{r}} = 8$, $\nu_{\mathfrak{a}} = 6$, $\nu_{\mathfrak{d}} = 3$, $\nu_{\mathfrak{f}} = 6$, $\beta_{\mathfrak{a}} = 4 \times 10^6\,\alpha_{\mathfrak{r}}$ $\beta_{\mathfrak{d}} = 4 \times 10^6\,\alpha_{\mathfrak{r}}$, $\beta_{\mathfrak{f}} = 4 \times 10^6\,\alpha_{\mathfrak{r}}$).

Figure 5 shows the outcome of simulations where adhesive contact forces (38) have been added. To better understand the influence of adhesive forces these simulations consist in computing the motion generated by throwing the body against

either a horizontal support (like a ceiling, Fig. 5 a) or a vertical support (like a wall, Fig. 5 b), in order not to confuse the adhesive forces with the gravity force. The initial velocity has been calibrated in such a way to let the body touch the support without bouncing back. Once the body has got stuck to the support, the mass density of the body is increased gradually as a trick to make the bond brake. And that is exactly what happens: the body detaches from the support and falls down.

The role of the friction is very different in the two simulations. While in case (a) the friction just slows down the body until it stops sliding on the ceiling, in case (b) the friction prevents the body from sliding down the wall until it suddenly starts detaching. The trajectory of the center of the body and a few frames help to understand the motion.

7.5 Bouncing and Vibrations of a Soft Body

For plane deformations it is convenient to enforce *a-priori* the incompressibility constraint $\det \mathsf{F} = (\det \mathsf{R})(\det \mathsf{U}) = 1$ by giving the matrix of the stretch U the following parameterized form

$$\begin{pmatrix} \frac{1+\kappa^2}{\chi} & \kappa \\ \kappa & \chi \end{pmatrix}. \tag{39}$$

The principal stretches λ and $1/\lambda$, turn out to be given by the expression

$$\lambda := \left(1+\kappa^2+\chi^2+\sqrt{(1+\kappa^2)^2+2(\kappa^2-1)\chi^2+\chi^4}\right)/(2\chi). \tag{40}$$

Denoting by θ the amplitude of the rotation R, the tensor F will be described by the three parameters: θ, κ, χ.

Figure 6 shows a cylinder, with diameter L, bouncing in a plane vertical motion, after dropping on the support from a distance v_0. In this case λ denotes the vertical stretch while $1/\lambda$ denotes the horizontal stretch, given by the ratio $l(t)/L$. Both friction and impact damping have been neglected. The motion described by the graphs in Figure 6 (b)-(c) is only slightly damped by a dissipative stress with a low value for the coefficient μ. It is worth noticing how the deformation of the body reflects on the bouncing. Comparing the time-histories of the center C and the bottom B (Fig. 6 b), we can see a sequence of bounces, due to the motion of the center, together with other bounces with a lower amplitude and a higher frequency, due to the stretching. The frequencies of the two kinds of bouncing seem to be far enough not to interact significantly with each other. The graphs in Fig. 6 (d)-(e) show the effects of a higher value for the coefficient μ, to be compared with the graphs above. After a short while the dissipation is able to slow down both the bouncing and the vibrations.

The body in Fig. 7 falls down on the support from a distance v_0 with an initial leftward horizontal velocity $\dot{u}_0$. The friction makes it start rolling while the impact is

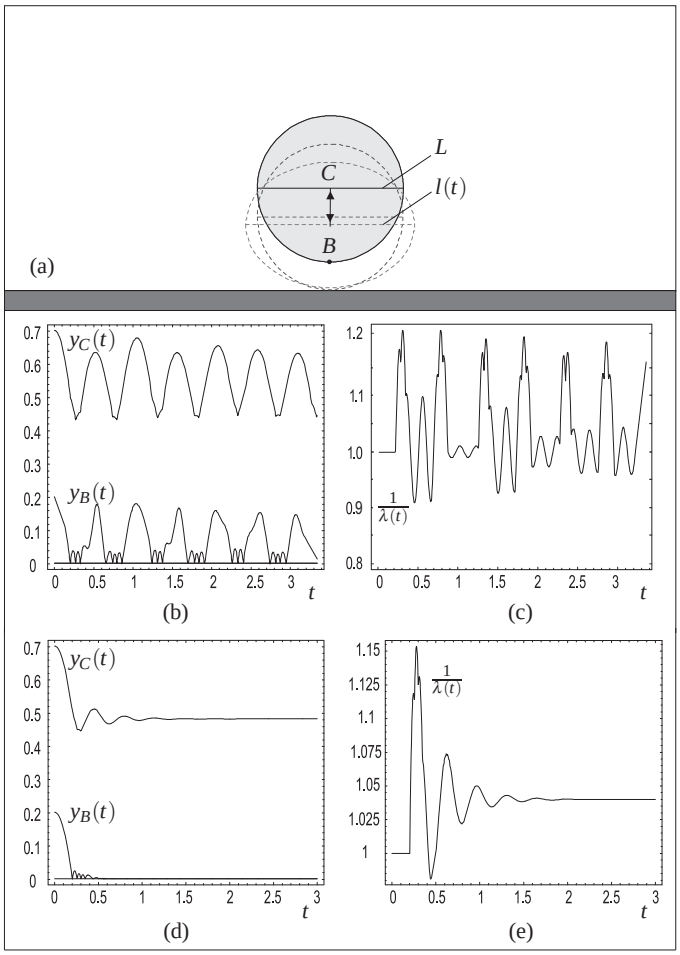

Fig. 6 Motion of an elastic cylinder ($L = 1\,\mathrm{m}$, $d_0 = 0.002\,\mathrm{m}$, $\nu_0 = 100\,d_0$, $c_1 = 6 \times 10^4\,\mathrm{Pa}$, $\rho = 4 \times 10^3\,\mathrm{Kg/m^2}$, $\nu_\mathfrak{r} = 8$, $\nu_\mathfrak{d} = 2$, $\nu_\mathfrak{f} = 2$, $\beta_\mathfrak{d} = 0$, $\beta_\mathfrak{f} = 10^9\,\alpha_\mathfrak{r}$, $\mu = 10^2\,\mathrm{Pa\ s}$): (a) selected frames; (b) distance of B and C from the support; (c) principal stretch; (d)-(e) effect of a higher dissipative stress ($\mu = 5 \times 10^3\,\mathrm{Pa\ s}$).

followed by a few bounces. The body is stiffer and heavier than the body in Fig. 6. The resulting vibration frequency is higher while it bounces almost at the same frequency.

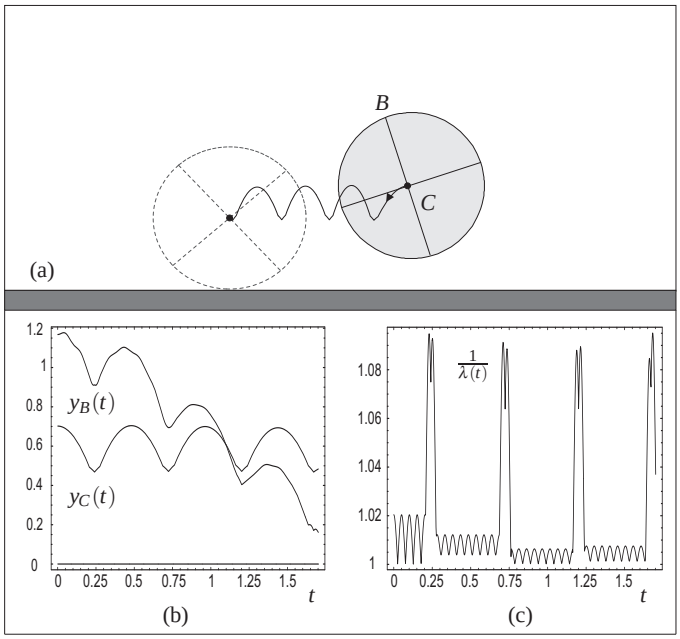

Fig. 7 Motion of an elastic cylinder ($L = 1\,\mathrm{m}$, $d_0 = 0.002\,\mathrm{m}$, $c_1 = 6 \times 10^6\,\mathrm{Pa}$, $\rho = 10^5\,\mathrm{Kg/m^2}$, $\nu_\tau = 8$, $\nu_\vartheta = 2$, $\nu_\mathfrak{f} = 2$, $\beta_\vartheta = 0$, $\beta_\mathfrak{f} = 10^7\,\alpha_\tau$, $\mu = 10^2\,\mathrm{Pa\ s}$, $v_0 = 100\,d_0$, $\dot{u}_0 = -1\,\mathrm{m/s}$).

7.6 Driven Motion of a Soft Contractile Body

Figure 8 shows the vertical motion of a contractile body driven by an oscillating external contractile couple Q. The contraction is assumed to be isochoric and with a fixed eigenvector $\mathbf{n}$, the external unit normal to the support. In such a motion G is described by a scalar time function γ, which is one of its eigenvalues together with $1/\gamma$. The couple Q is described by a scalar function as well, which has been assigned the law $Q(t) = Q_0 \sin(2\pi t/T)$, with $T = 0.4\,\mathrm{s}$, $Q_0/\mu_\gamma = 0.9\,\mathrm{s}^{-1}$. The resistance to contaction μ_γ was set to a very high value in order to prevent plastic deformation or relaxation induced by the stress and the energy terms in (24). The body initially lies at rest on the support, slightly deformed by its weight. As soon as the signal is activated the body starts oscillating and, as can be noticed in the selected frames in Fig. 8 (a)-(b), and from the graph (d), it contracts and jumps upward. The evolution of the relaxed shape is shown in Fig. 8 (c). The graph in Fig. 8 (e) describes the time evolution of the vertical elongation $(\lambda(t)\gamma(t) - 1)$, which is compared with $Q(t)$.

Figure 9 shows a motion driven directly by an oscillating tensor G. The contraction is assumed again to be isochoric and is assigned by the eigenvalue law $\gamma(t) = 1 + (\gamma_0 - 1)\sin(2\pi t/T)$, with $T = 1.1\,\mathrm{s}$, $\gamma_0 = 1.2$, and by a rotating eigenvector $\mathbf{a}(t)$, with a constant angular velocity $(0.8\,\pi/T)$. It is worth noting that $\mathsf{G}(t)$ at any time t is a symmetric tensor with positive eigenvalues. Hence G does not

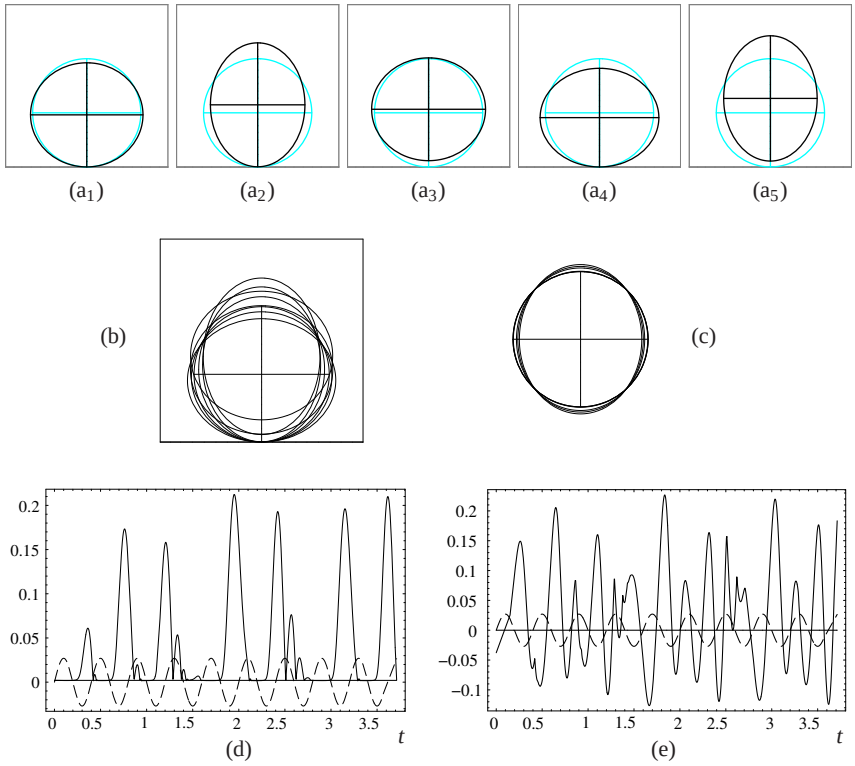

Fig. 8 Motion generated by an oscillating contractile couple with fixed principal axes: (a) selected frames showing how the body jumps upward; (b) overlapped body shapes during the motion; (c) oscillating relaxed shape; (d) bouncing of the bottom over the support, and driving contractile couple Q (dashed line, rescaled amplitude); (e) vertical elongation (solid line) and driving contractile couple Q (dashed line, rescaled amplitude).

generate a rotating relaxed shape but just a pulsing relaxed shape with varying pulse axis (Fig. 9 c). The body starts oscillating and soon, from an initial configuration on the right side of Fig. 9 (a), it moves leftward rolling, almost crawling, and even jumping a little. In Fig. 9 (d) the increasing horizontal displacement of the center C and of the bottom B in the starting configuration are showed together with the oscillating driving contraction.

As expected, locomotion on a support relies on the frictional traction: removing the friction the body cannot move forward any more while the center follows a vertical trajectory (Fig. 9 b).

The contractile couple Q, which was a given quantity in the previous case, can now be computed through (24), as a reactive couple. In both cases the power expended per unit volume to sustain the body motion is $\mathsf{Q} \cdot \dot{\mathsf{G}}\mathsf{G}^{-1}$.

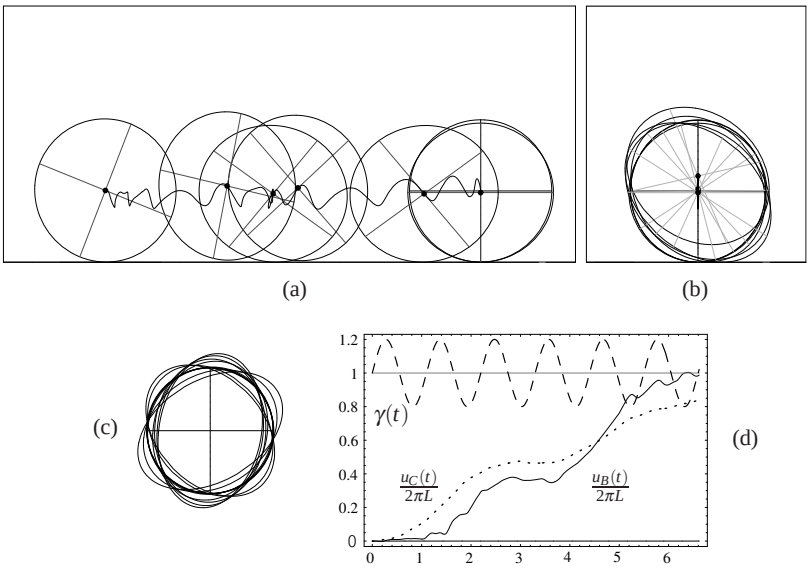

Fig. 9 Motion driven by an oscillatory contraction with rotating principal axes: (a) trajectory of the center and some frames from right to left; (b) frictionless motion; (c) the oscillating relaxed shape; (d) normalized leftward displacement of the initial bottom point B (solid line) and of the center C (dotted line), and driving contraction amplitude (dashed line).

8 Conclusions

The aim of this paper was to study the motion of a soft contractile body over a rigid substrate. To this end a non linear elastic model has been used together with a contact model based on constitutive laws for different kind of interactions. The body model, though restricted to homogeneous deformations, accounts for large deformations and also for an evolving relaxed shape. This makes it possible to give a precise meaning to contractility. The constitutive characterization of both the material and the contact is based on a purely mechanical dissipation principle which enlighten the role of energy functions for both stress and contact forces. The presented simulations are meant to illustrate the realizable motions, in the presence of contact interactions, like repulsion, adhesion, impact damping and friction, of a body with different material properties, showing the interplay between contact, vibrations and contractions. In particular it is shown how the contractility endows a body with motility capabilities which can be exploited for locomotion. All the computations, both symbolic and numerical, have been performed using *Mathematica*®, starting from the very basic expressions in sections 2, 3 and 4. Further work should be done for gaining better physical interpretations of numerical simulations by using parameters based on experimental data and by comparing results with other models.

References

1. Argento, C., Jagota, A., Carter, W.C.: Surface formulation for molecular interactions of macroscopic bodies. J. Mech. Phys. Solids **45**, 1161–1183 (1997)
2. Contento, A., Di Egidio, A., Dziedzic, J., Tatone, A.: Modeling the contact of stiff and soft bodies with a rigid support by short range force fields. TASK Quarterly **13**, 1001–1027 (2009)
3. Di Carlo, A., Quiligotti, S.: Growth and balance. Mech. Res. Comm. **29**, 449–456 (2002)
4. Gao, J., Luedtke, W.D., Gourdon, D., Ruths, M., Israelachvili, J.N., Landman, U.: Frictional forces and amontons? law: From the molecular to the macroscopic scale. J. Phys. Chem. B **108**, 3410–3425 (2004). DOI 10.1021/jp036362l
5. Germain, P.: The method of virtual power in continuum mechanics. Part 2: Microstructure. SIAM J. Appl. Math. **25**, 556–575 (1973)
6. Greenwood, J.A.: Adhesion of elastic spheres. Proc. R. Soc. Lond. A **453**, 1277–97 (1997). DOI 10.1098/rspa.1997.0070
7. Gurtin, M.E.: A gradient theory of single-crystal viscoplasticity that accounts for geometrically necessary dislocations. J. Mech. Phys. Solids **50**, 5–32 (2002)
8. Johnson, K.L., Kendall, K., Roberts, A.D.: Surface energy and the contact of elastic solids. Proc. R. Soc. Lond. A **324**, 301–313 (1971). URL http://www.jstor.org/pss/78058
9. Mogilner, A.: Mathematics of cell motility: have we got its number? J. Math. Biol. **58**, 105–134 (2009)
10. Muller, V.M., Yushchenko, S., V., Derjaguin, B.V.: On the influence of molecular forces on the deformation of an elastic sphere and its sticking to a rigid plane. J. Colloid Interface Sci. **77**, 91–101 (1980). DOI 10.1016/0021-9797(80)90419-1
11. Nardinocchi, P., Teresi, L.: On the active response of soft living tissues. J. Elasticity **88**, 27–39 (2007)
12. Sauer, R.A., Li, S.: A contact mechanics model for quasi-continua. Int. J. Numer. Meth. Engng **71**, 931–962 (2007)
13. Sauer, R.A., Wriggers, P.: Formulation and analysis of a three-dimensional finite element implementation for adhesive contact at the nanoscale. Comp. Meth. Appl. Mech. Engng. **198**, 3871–3883 (2009)
14. Spolenak, R., Gorb, S., Gao, H., Arzt, E.: Effects of contact shape on the scaling of biological attachments. Proc. R. Soc. Lond. A **461**, 305–319 (2005)
15. Wriggers, P.: Computational Contact Mechanics. John Wiley & Sons (2006)
16. Yu, N., Polycarpou, A.A.: Adhesive contact based on the Lennard-Jones potential: a correction to the value of the equilibrium distance as used in the potential. Journal of Colloid and Interface Science **278**, 428–435 (2004)